Highlights

Edge Computing Design Space Exploration for Heart Rate Monitoring

Jose A. Miranda, Manuel F. Canabal, Laura Gutiérrez-Martín, José M. Lanza-Gutiérrez, Celia López-Ongil

- Design Space Exploration is an essential task when facing the development of physiological edge computing devices.

- The different morphology of PPG signals directly affects the data processing chain of HR-based wearable devices.

- Heart Rate Variability is a reliable metric to detect physiological activation.

Edge Computing Design Space Exploration for Heart Rate Monitoring

Jose A. Miranda[a], Manuel F. Canabal[a], Laura Gutiérrez-Martín[a], José M. Lanza-Gutiérrez[b], Celia López-Ongil[b]

[a]*Electronic Technology Department, Carlos III University of Madrid, Leganés, Comunidad de Madrid, Spain*
[b]*Department of Computer Science, University of Alcalá, , Alcalá de Henares, Comunidad de Madrid, Spain*

Abstract

Edge computing, smart sensors, and health monitoring are boosting current wearable development and enabling the next technological user-centered revolution. Within this context, high added value applications based on physiological information are gaining attention during the last years. Among the vast physiological metrics available, heart rate variability (HRV) is one of the most used, from which different types of information related to the activity of the autonomic nervous system can be obtained. This fact has led integrated chip manufacturers to foster the design of novel analog front end circuitry for heart rate monitoring, which has forced a wearable smart sensor innovation. Notwithstanding the capabilities and efficiency of these novel sensors, different design space exploration (DSE) procedures must be addressed for every sensor integrated within a wearable system towards maximizing the embedded resources usage. On this basis, this paper presents an exhaustive DSE in-depth study for every stage affected in a wearable edge device developed by the authors and based on HRV physiological monitoring. The particulates of such system are detailed and explained. Moreover, time complexity and memory usage comparison regarding different digital signal processing techniques are provided, which results in a set of recommendations for wearable constrained application needs. Finally, a use case is presented based on a rapid stress detection application by using the different DSE recommendations for our specific wearable edge device. This application reaches adequate trade-off precision for detecting physiological HRV activation by using only four second temporal processing window.

Keywords: edge computing, heart rate, wearable design, design space exploration

1. Introduction

In the last decade, academic and industrial research on wearable affective computing and emotion recognition has gained attention [1]. Among the smart sensors considered for wearable affective computing, physiological sensors such as heart rate (HR), skin temperature (SKT), and electrodermal activity (EDA) are those that provide a seamless implementation from current commercial-off-the-shelf (COTS) devices. Within this physiological context, the autonomous nervous system (ANS) controls the physiological regulation produced by affective states [2]. Thus, unlike other types of information, such as voice or gestures, physiological signals can not be controlled by humans, resulting in reliable information to identify any emotional change. Different public and private databases dealing with emotion recognition and wearable integration were developed in last years [3]. These and other related experiments performed different signal processing and feature extraction stages in an offline manner, meaning that the wearable device was only considered to collect data. This situation implied that they did not need to address the design space exploration (DSE) within their wearable embedded devices to optimize computational time or memory usage. However, when designing a wearable edge device for online physiological monitoring being able to deal with complex stages as data acquisition, processing, and feature extraction, a detailed DSE must be performed to ensure that the hardware resources available are successfully exploited.

Nowadays, there is a wide range of analog front end (AFE) solutions for smart sensors, which provide enough independence and autonomy to not overload the connected microcontroller unit (MCU) with tasks such as acquisition, data filtering, and even data processing. However, there exist open questions related to the management of the quality and quantity of the information provided by the sensors, that affect the performance of the different algorithms to be integrated into the MCU. Thus, obtaining enough useful information is essential and subjected to both the AFE and the main device capabilities (processing and storage).

Other open questions are related to energy cost and operating lifetime, which are critical aspects specially in wearable constrained devices. All these open questions can be addressed by performing application and platform-oriented DSEs, prior to integrating the components into the wearable edge device. Moreover, one of the main principles to be considered when designing a low-resource wearable edge computing device for physiological monitoring through the integration of smart sensors is related to the form factor. This fact should be considered essential from an unobtrusive design perspective. For instance, several physiological-based computing systems were proposed in the literature [4], but most of them were based on laboratory setups. That means that these systems included sensors such as electrooculogram, electromyogram and electroencephalogram, among others, hindering the current wearable-ready feasibility. This latter fact is explained by the not-ready current technological inconspicuous aspect of such sensors.

From a physiological point of view, a deep understanding regarding the ANS behaviour is needed when dealing with these systems and this type of information. For instance, the relationship between both branches of the ANS, i.e., sympathetic nervous system (SNS) and parasympathetic nervous system (PNS), is usually explained by considering HR and heart rate variability (HRV), which is the temporal inter-beat-interval (IBI) or the time difference between successive HR beats. When dealing with stressful situations, the SNS increases HR, which leads to a more constant HRV. On the other hand, in a relaxed affective state, the PNS decreases the HR, which produces a more variant HRV [5]. Currently, HR and all the metrics extracted from it are widely used in the literature due to the direct relationship with emotions and physiological states [6]. These metrics can be derived from electrodes placed on the skin (electrocardiogram or ECG) or from blood volume pulse (BVP) changes by using a photoplethysmogram (PPG) sensor, presenting the latter more wearable possibilities than the former. It should be noted that a valid surrogate of HRV is the peak rate variability (PRV) from BVP [7].

Different HR-based wearable edge computing systems tried to link the wearable embedding restrictions to the performance of the machine learning to be implemented inside. Most of the works did not present a detailed DSE to support design decisions. In [8], the authors presented an ultra-low-power wearable system with deep learning capabilities based on ECG information. This work was the first paper dealing with the study of wearable embedded edge computing-based emotion recognition capabilities. They considered a COTS ARM®Cortex®-M4F MCU and provided a partial DSE based on the performance of a lightweight artificial neural network. Nonetheless, they did not consider the volatile memory usage. Other approaches using more powerful platforms were also published. In [9], the authors considered the Intel Galileo board and provided the Pareto optimal solution for a DSE based on arrhythmia accuracy detection and computational cost. Nevertheless, they leave memory impact analysis aside, which could be due to the high performance of the board with 400MHz clock speed and 256MB RAM. Other parameters for the DSE could be defined based on the application, for instance, the authors in [10] considered a wearable watch based on ARM®Cortex®-M MCU and performed their DSE based on the number of detected ECG beats, but without providing any computational cost or memory impact analysis.

When designing a HR-based wearable edge computing system, the digital data processing stages include from the instant of raw signal acquisition, filtering, motion artifact removal, peak identification, interpolation, and power spectral estimation, to the instant before the inference process by the machine learning engine. Each of these stages can be subjected to individual DSEs based on available resources and time requirements, among other application parameters. Thus, this paper aims to provide a detailed DSE of the main embedded procedures needed to implement this type of physiological wearable systems. To accomplish this work, the authors consider the BINDI wearable affective computing platform [11, 12]. Note that this paper is an extended version of [13]. In this version more technical information regarding filtering, PPG morphology and peak detection algorithm comparison is included. The main contributions of this work are as follows:

- Implementation and study of a detailed DSE for the main stages involved in a physiological based wearable edge computing device based on an ARM Cortex®-M4 processor.
- The use of experimental results to show the performance of the concluded trade-offs regarding the amount of physiological activation information detection.
- Evaluation of a complete data processing chain for real physiological based wearable into an ARM Cortex®-M4.

The rest of the paper is organized as follows. Section 2 presents the hardware and software architectures of the wearable system. Section 3 discusses the DSEs

for the different stages and exposes the results obtained. Section 4 presents a specific rapid physiological activation detection application use case by considering the results given by the DSEs. Finally, conclusions and future works appear in Section 5.

2. System Architecture

BINDI is a wearable solution, composed of a bracelet, a pendant, and a smart-phone application, whose final goal is detecting gender-based violence situations by using affecting computing [14]. This work focuses on the bracelet subsystem, which is equipped with three physiological sensors: EDA, SKT, and BVP. The data provided by these sensors together with a comprehensive signal processing and a lightweight machine learning engine are embedded within the bracelet MCU. The next subsections describe the bracelet hardware and software architectures subjected to analysis in this document.

2.1. Bracelet Hardware Architecture

The hardware architecture in the BINDI bracelet is formed by the MCU, the physiological sensors, and other necessary elements, such as a Power Controller Unit (PCU), which handles the battery consumption and correctly supply the MCU and sensors. Next, specific details about these parts are as follows:

- **MCU:** nRF52832 SoC ARM®Cortex®-M4 32-bit, with 64MHz clock speed, 512KB memory flash, 64KB RAM, single-precision floating-point unit, Thumb®-2 instruction set, Bluetooth Low Energy 5.2, and some integrated peripherals (UART, SPI, I2C, I2S, RTC, PDM, AES).
- **PCU:** BQ2407xT and MAX17055 are responsible for charging and monitoring the battery. Both integrated circuits are intended for low-power handheld and/or wearable devices. They are accompanied by a set of different low-dropout regulators to power-on the different parts of the bracelet.
- **Physiological sensors:** The only physiological sensor of interest for this work is the BVP sensor. That is the MAX30101 High-Sensitivity reflective pulse-oximeter and HR Sensor for wearable health, with configurable sampling frecuency from 50Hz up to 3.2kHz, integrated LEDs (red, green, and infrared), noise cancellation, 18-bit current ADC, and I2C communication.

2.2. Bracelet Algorithmic Architecture

2.2.1. Data Segmentation

Although it is possible to extract real-time information from HR information [15], data partitioning is needed when dealing with wearable constraint devices. Moreover, physiological data segmentation and overlapping are recommended to enhance the physiological stimuli classification from an affective computing perspective [16].

During this process, the raw signal data is acquired based on a temporal window requirement. The length of the window, the number of windows, and the existence of window overlapping will depend on the capabilities and specifications of the system, as well as the application.

2.2.2. Data Processing

The goal of this stage is to eliminate all the undesired frequency components within the signal, being essential because PPG signals are specially sensitive to noise. There are two main tasks in this stage: filtering and motion artifact removal (MAR), being both widely addressed for wrist-worn devices in the literature [17].

Filtering. Filtering aims to eliminate all unnecessary frequencies by applying digital filtering techniques. One of the most common approaches is considering bandpass filtering, leaving wide enough bandwidth to detect any possible HR frequency. For instance, from 0.5Hz (30 BPM) to 4Hz (240 BPM). From an embedded or a digital perspective, there are two main techniques for this filtering process: infinite impulse response filters (IIRs) and finite impulse response filters (FIRs). IIRs are computationally fast, although it does not have a linear phase response, which could lead to not preserving the wave-shape, resulting in wrong affective patterns to be identified by the intelligence engine. This disadvantage is avoided by using a forward-backward IIR filtering [18] technique, which requires double filtering and double time reversal of the signal. This latter fact leads up to higher computational time at the expense to obtain a zero-phase transfer function using IIRs. On the contrary, FIR filters can be designed to have a linear phase response, so preserving the wave-shape and not affecting possible patters. Although they require more coefficients and memory than IIRs, they do not need to perform the amount of operations as for forward-backward IIR filtering. These and other digital techniques are used to deal with out-of-band noises, such as baseline wander and high frequency noise. The former is related to low-frequency disturbances, bellow 0.5Hz,

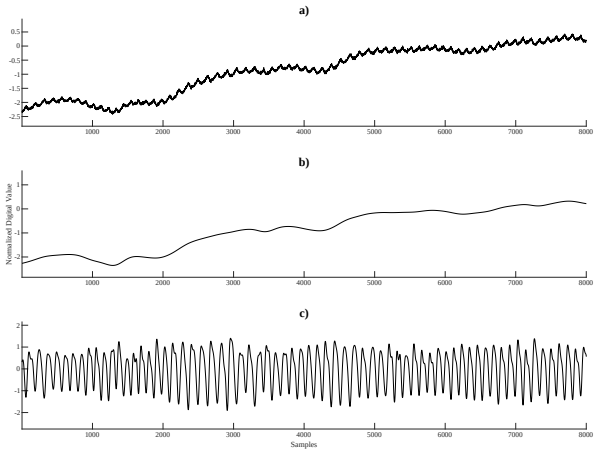

Figure 1: Example of different noise sources for PPG: a) raw PPG contaminated by baseline wander and high frequency noise, b) extracted baseline wander by applying a forward-backward IIR filtering, c) PPG filtered signal without any out-of-band noise.

while the latter is due to typical electrical noise. For instance, Figure 1 shows the effect of these two types of noises over raw PPG data. The rejection of these types of noises is key to properly minimize changes in PPG signals morphology that does not have a cardiac origin.

Motion artifact removal. MAR techniques aim to detect and remove transient changes because of movements of areas where the sensor is placed, which are translated into in-band noises. These types of techniques are quite computationally demanding, worsening their applicability in wearable devices. This fact makes the design of lightweight MAR techniques be a hot topic nowadays. The different solutions to deal with this problem range from the use of adaptive filtering by using a surrogate set of signals, e.g., inertial motion unit signals [19], to the use of extensive matrix operations, e.g., singular value decomposition with different PPG wavelength sources [20]. The comparison and implementation of different MAR techniques are not within the scope of this work.

2.2.3. Feature Extraction

The goal of this stage is to extract useful information from the data obtained in the previous stage. The first step consists in calculating the HRV for the current temporal window. To this end, it is required to get the IBI along with the window by detecting different peaks of the PPG signal. The robustness of this delineation process is key to properly detect the desired morphological PPG parameters. This fact is determined not only by the previous filtering step but also by the different

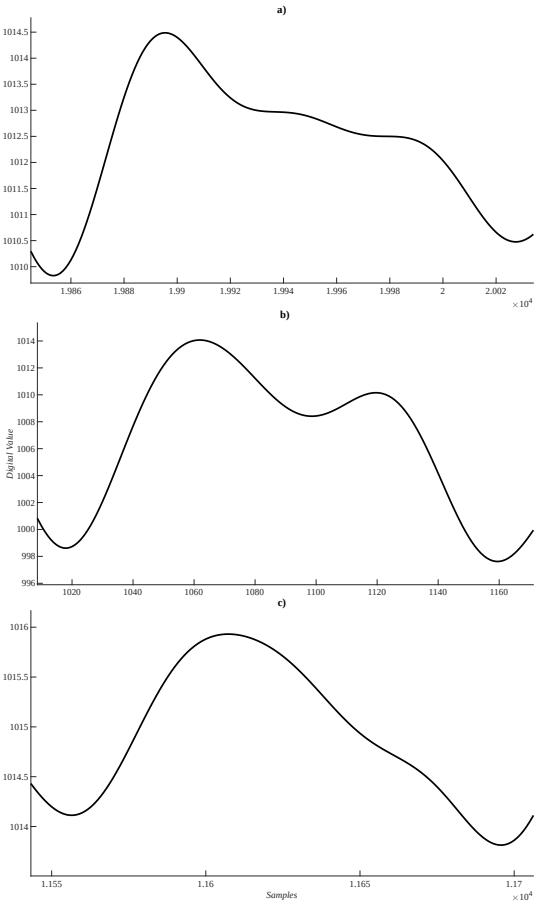

Figure 2: PPG morphological differences between three age groups: (a) 18-24 year old person, (b) 35-44 year old person and (c) 55-65 year old person.

PPG wave morphologies, which can be directly affected by factors such as age and emotions [21, 22]. Figure 2 shows the morphological difference between three different age groups measured with our PPG sensor. The differences observed are in line with the ones published in the literature [23]. For instance, the dicrotic part of the wave is the most affected. This is mainly due to the vascular tone variation with age, which is directly translated into more or less vasoconstriction and vasodilation. This fact produces differences in arterial pressure leading to distorting diastolic run-off.

Within this physiological variable context, different algorithms could provide different delineation results, also affected by the previous filters applied. For instance, if the application does not use any baseline wander removal filter, e.g. notch filter bellow 0.5Hz, the different points extracted by the delineation algorithm employed should be robust enough to not be affected by the low-frequency out-of-band trends. Different tech-

niques can be applied to assure robust peak-to-peak detection, however, some of them require the implementation of zero-crossing throughout the first and second derivatives of the signal [24, 25]. This fact directly affects the computational time within the data processing chain. Therefore, the authors consider the implementation and comparison of two different PPG algorithms. On the one hand, the first is based on a local maximum/minimum method (LCM) developed by the authors using the local slope and mean evolution over short periods of samples along with the data processing window. LCM methods are well known within PPG peak detection algorithms as they used to be less computationally demanding at the expense to lower performance. On the other hand, the second algorithm is taken from [26], which is based on an adaptive threshold detection method (ADT) that outperformed LCM techniques without requiring first and/or second derivative signal operations. Note that the latter algorithm has been validated against publicly available datasets.

Once the delineation is performed and the HRV is calculated for the current window, several statistical, frequency, and non-linear features can be derived from this information. Among them, frequency ones are specially interesting because they provide information about SNS and PNS activation in form of four bands: 0.01-0.04Hz, 0.04-0.15Hz, 0.15-0.40Hz, and 0.40-1.00Hz. As they are very low frequency bands, obtaining information with enough resolution with physiological-based wearable devices is still challenging.

3. HR-Based Design Space Exploration

To achieve a full wearable integration, individual DSEs are recommended for the sensors in the system. These DSEs could focus on the quality of the output obtained for each stage in the software architecture involving the sensor. This section presents a HR-based DSE focused on extracting HRV frequency information. This DSE is split into the different stages in the software architecture, as Fig. 3 shows.

3.1. Data Segmentation: Windowing and Overlapping

Data acquisition and temporal storage are key tasks when dealing with wearable constrained systems for continuous rapid inference applications. Enough processing time between acquisitions must be assured to perform the rest of the data processing chain.

Time and memory requirements linearly increase with the length of the window and the sensor sampling frequency. Different trade-offs must be taken at

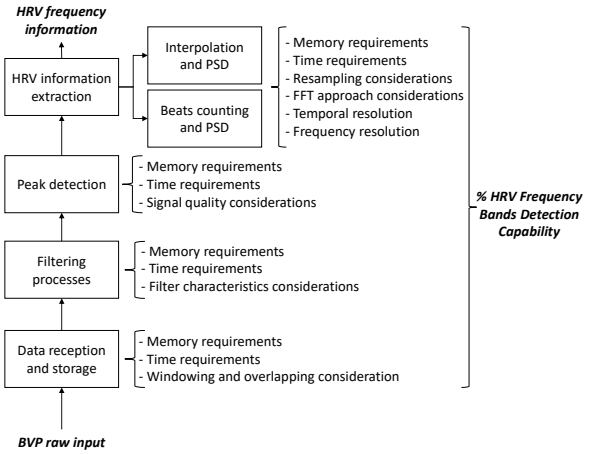

Figure 3: Parameters and processes involved in the BVP-based DSE.

this stage considering how many information and how frequently is needed. For HRV, this fact is challenging because HRV information is an unevenly or non-uniformed sampled signal, because human cardiac frequency is not constant. The number of HRVs susceptible to be detected into one window is given by

$$HRV_{W_i} = \frac{W_L}{T_{HR_i}} - 1, \tag{1}$$

where W_L is the window time duration, T_{HR} is the period of the current HR, and i is the window number. This equation is applicable for fixed windowing strategies. However, this scheme suffers from a variable temporal and frequency resolution problem. Suppose that an application requirement is to give a response on every processed window, then the amount of information in each window will not be the same. Different alternatives can be used to avoid this problem, from interpolation to even dynamic frequency resolution adjustments if the application allows it. Another approach is to work with dynamic window length and overlapping. Although, this type of allocation is intended to optimize resources, a memory handler should be designed to manage all the allocations and deallocations performed. The latter leads to more added ROM memory usage and computational time.

Regardless of the windowing and overlapping lengths, data processing must be performed between window acquisitions. If the MCU is fast enough to perform the data processing from a window before acquiring the next one, then only one buffer is required. However, this is not usual in constrained devices, so two buffers are commonly included, i.e., one for data acquiring and the other for data processing.

3.2. Data Processing: filtering

The authors consider five parameters for the filtering DSE: memory usage, window computation time, settling time, stop-band mean attenuation, and bandpass ripple. The two first parameters are related to the filter implementation and are constrained by the microcontroller resources. The computation time parameter is also constrained by the timing defined by the application. The other parameters are related to filter characteristics. Settling time is specially relevant denoting the filter stabilization time, which could be linked with a waste in time and memory. Stop-band mean attenuation is related to the mean attenuation level with the designated rejection band, while bandpass ripple is the amount of variation in the gain within the designated bandwidth of the filter.

Four filter design options are considered, three bandpass FIR filters with different orders and a two-stage filter based on moving averaging. The design of bandpass filters was conducted by Matlab® according to the equiripple method. The resulting coefficients were quantified to 14-bit integer to reduce memory usage and boost processing time. This number of bits is the maximum precision that ensures no overflow in this system, with 18-bit BVP signals and 32-bit registers. The frequency response impact is minimal and the root means square deviation of the output compared with 64-bit floating-point coefficients is less than 0.6. On the other hand, the two-stage filter is composed of two moving averaging steps. The first one is a low pass 4-sample filter. The second one is the signal subtraction of the 100 values, centered moving average.

Table 1 shows the result obtained for the filtering DSE. Analyzing this table, the authors reach that, for bandpass filters, increasing the filter order (the number of coefficients) increases mean stopband attenuation but also ROM memory usage, computation time, and settling time. The computation time for these bandpass filters could be reduced if coefficients are stored in RAM at the expense of memory usage. Note that the computation for the two-stage filter is significantly lower than for the bandpass filters.

Regarding stopband attenuation, this parameter benefits bandpass filters, providing a higher attenuation across all the stopband. Note that the most efficient relationship stopband attenuation vs. ROM memory usage is reached by the 400-coefficient bandpass filter, because of the constant code size effect. Focusing on the bandpass ripple, this metric remains below limits in all cases but especial care should be taken in the rest of the processing chain if the third bandpass filter is implemented. Regarding settling time, the difference between two-stage and bandpass filters is large, benefiting the latter. From all this analysis, the authors select the two-stage filter, with a good trade-off between computation time, attenuation, and memory usage.

Table 1: Results obtained for the DSE filtering.

Desing options	Compt. Time [ms]	RAM [bytes]	ROM [bytes]	Set. Time [samples]	Mean stopband att. [dB]	bandpass ripple [dB]
400-coef	0.2474	10	626	400	-38.8	0.09
200-coef	0.1240	10	426	200	-25	0.64
100-coef	0.0623	10	326	100	-14.9	3.09
2-stage	0.0048	20	470	4	-9.3	1.93

3.3. Feature Extraction: Peak Detection

As commented in Section 2.2.3, different approaches can be used to delineate PPG time series. In our particular case, a computational comparison between two well-known approaches is presented. The first algorithm implemented, Algorithm 1, is based on LCM techniques, while the second algorithm uses an adaptive threshold through a varying slope.

Figure 4 shows a time impact analysis for the two different peak detection algorithms considering the number of samples in the processing window. For the LCM algorithm, the number of samples to be compared within the slope and the mean local evaluation (*stc*) is the key element. Note the high time complexity of this type of time series processing, as every sample of the signal needs to be evaluated against its neighbors. For instance, if the BVP signal is sampled at 100Hz, the mean evaluation over ten samples supposes -6dB attenuation for 6Hz and -3dB attenuation for 4.5Hz, being the latter close to 4Hz which is a frequency of interest, as stated in Section 2.2. Thus, based on the residual high noise frequencies of the signal filtered, this parameter can be adjusted. For this particular algorithm, and guided by the trade-off taken on the previous stage, a *stc* equal to ten can be chosen, which increases peak detection capabilities at the expense of time complexity. The LCM algorithm used is one of the simplest, yet it fits the requirements of our particular use case. Moreover, the implemented algorithm just utilizes 2KB of ROM and 16B of RAM. On the other hand, regarding the ADT algorithm, there can be observed a computational time increase between 30% and 50% in comparison to an LCM algorithm with the highest *stc*. This fact is mainly due to the calculation of the standard deviation for the whole processing window signal, which is needed for obtaining the varying slope to be used by this algorithm. In this case, 2.5KB of ROM and 64B of RAM are used by this algorithm.

Algorithm 1: BVP Peak Detection Algorithm

function getPeaks (bvp_{signal}, bvp_{len});
Input :
Clean BVP signal bvp_{signal};
Total number of samples bvp_{len};
Output:
Detected peaks position $peaks_{index}$;
Total number of peaks $peaks_{total}$;
$peaks_{max} \longleftarrow 0$;
$peaks_{min} \longleftarrow 0$;
for $i \leftarrow 1$ **to** $(bvp_{len} - stc)$ **do**
  $peaks_{index}(i) \longleftarrow 0$;
  if $bvp_{signal}(i) > peak_{max}$ **then**
    Check not finished valley detection;
    $vtc_{mean} \longleftarrow$ mean value for $i+stc_{min}$;
    Check consecutive identical points;
    $vtc_{slope} \longleftarrow$ slope for i and stc_{max};
    if $vtc_{mean} \geq peak_{max}$ **then**
      if $vtc_{slope} < 0$ **then**
        Last point of a peak found;
      end
    else
      Check if a peak was already detected;
      if *peak not detected* && $vtc_{slope} < 0$ **then**
        A peak was left behind;
      end
    end
  end
  if $bvp_{signal}(i) < peak_{min}$ **then**
    Perform opposite operation to detect valleys;
  end
end

3.4. Feature Extraction: HRV Information

In digital constrained embedded systems, frequency analysis are performed by DFT. One of the usual algorithms is the Fast Fourier Transform (FFT). However, this algorithm is based on the assumption of an equidistant sampled input. At this point, two possibilities arises based on the application needs. If the application is not limited by any inference time restriction, the system can wait until enough HRV points are extracted and the desired frequency resolution is possible. On the contrary, when continuous rapid inference is needed within a fixed temporal window, interpolation between the HRV samples is applied to reestablish the temporal coherence.

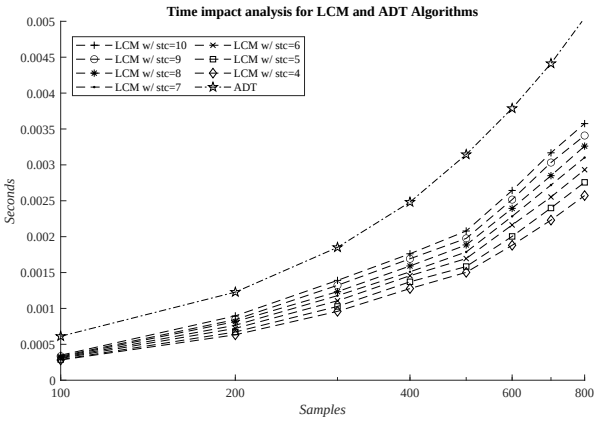

Figure 4: Time impact analysis for the peak detection algorithms.

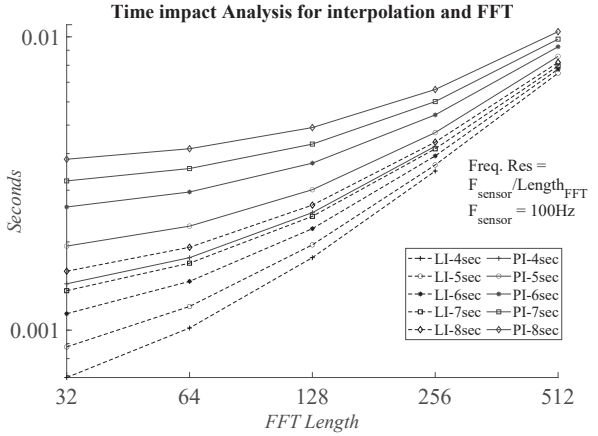

Figure 5: Time impact analysis based on different interpolation (Linear and Polynomial) methods.

Focusing on the continuous rapid inference use case, Fig. 5 shows a time impact analysis for different interpolation methods (linear and polynomial) and window processing lengths. As expected, polynomial methods have a higher time complexity, although producing more precise results if spectral accuracy is needed. Note that Lagrange polynomial interpolation is applied. In this particular case, a fixed-point 32-bit radix-2 FFT algorithm[1] is used, which provides one of the lowest computational complexities ($O(n \log n)$) and is then adequate for the embedded device.

In this stage a trade-off between temporal and frequency resolution must be taken. Note that independently of the f_{sensor}, if the window processing length is fixed, the frequency bin resolution for the chosen FFT_{len} will not change. Thus, in order to improve

[1] https://github.com/stg/SYLT-FFT

frequency resolution for a fixed temporal window, resampling techniques are applied after interpolation in these situations. For instance, if the HRV is interpolated at 100Hz for a fixed four second time window, it results into a 0.39Hz/bin resolution. However, after applying a 1Hz resampling, frequency resolution increases up to 0.25Hz/bin. Note that for the former case, only 256 available points are taken. In case of taking more points than the window length, zero padding must be applied. Thus, time and frequency resolution, as well as interpolation and resampling techniques, depend on the application. This is a key aspect when dealing with applications that require HRV frequency information extraction, as the lowest band of interest is located within 0.01Hz and 0.04Hz. Therefore, to achieve full HRV frequency band detection capability a minimum of 0.04Hz/bin should be assured. A frequency resolution value higher than that will decrease such detection capability. Note that frequency bin resolution is given by

$$f_{res} = \frac{f_{sensor}}{FFT_{len}}, \tag{2}$$

where f_{sensor} is the sampling frequency of the sensor, and FFT_{len} is the amount of samples of the processing window. Regarding temporal resolution, there must be considered that, based on Equation (1), the duration of the processing window must be selected to assure the presence of at least two HRV points, otherwise, interpolation is not possible.

Related to the memory storage considerations of this stage special care needs to be taken for FFT resource requirements by implementing in-place properties and non-recursive behavior. Resampling consumed resources are considered negligible. In our particular case, the interpolation utilizes 698B of ROM and 10B of RAM, while the FFT needs 3KB of ROM and 548B of RAM.

4. DSE Use Case Implementation

To give a real use case and implement all the different trade-offs concluded in each DSE stage, a specific four second stress rapid-inference application is presented. BINDI bracelet is programmed with all the detailed signal processing architecture and taken trade-offs. Thus, the HRV metrics for this application need to be extracted within the specified time. In this case, an experiment with six volunteers and ten different stressed and non-stressed one-minute audiovisual stimuli was used. These stimuli were previously labelled and selected by the authors. After each stimulus, the volunteers self reported their own level of arousal or excitement felt when watching the video. To provide a validation tool or a golden measure against the signals acquired by our platform, BioSignalPlux[2] was considered, which is one of the commonly employed professional physiological sensing systems for validations.

For this experiment, a 100Hz f_{sensor} was used and a fixed four second temporal processing window was employed. Note that for HRs bellow 45BPMs, this window is not applicable, as only one HRV point could be found. Every four seconds, the HRV points are extracted and interpolated, which is followed by a FFT calculation and a PSD estimate given by

$$PSD_i = \frac{2 * |fft|}{s}, \tag{3}$$

where PSD_i is the power spectral density for one specific frequency bin i, $|fft|$ is the squared spectrum magnitude and s is the sum of squared samples of the window function used. Specifically, to deal with scalloping loss and picket fence effects, a flat top window is applied. A fix FFT_{len} of 256 points is used, leading to a 0.39Hz/bin resolution. This resolution is enough to observe the activity of lower frequency bands (up to 0.4Hz) and higher ones (from 0.4Hz up to 1Hz). Take into consideration that in case of having less than 256 points after interpolation, zero padding is applied. The same digital procedure is applied for the validation tool and BINDI.

Table 2 shows the collected results obtained for two arbitrary selected stress (H) and non-stress (L) stimuli for the six different volunteers. $\overline{P}_{Gf1}$ is the averaged quotient between the first frequency bin (0.39Hz) and the second frequency bin (0.78Hz) during the stimulus using the signal from the validation tool, while $\overline{P}_{Gf2}$ is the one observed for the averaged quotient between the second frequency bin and the sum of the first and the second. The fourth and the fifth columns are the analogue values taken from BINDI. These results show a decrease on the first factor for all the patients from the stress to the non-stress stimulus. Conversely, there is a increase in the second factor. This is in line to the theory of the ANS. As commented in Section 1 and Section 2.2.3, the lower frequency bands are dominated by the SNS which is in charge of regulating stress situations, while PNS is related with the higher bands and responsible of controlling relaxed conditions. The errors between the validation results and BINDI results are also provided in Table 2 . These errors are low ($\varepsilon < 10\%$),

[2]https://www.biosignalsplux.com/index.php/researcher

Table 2: Measurement result of specific HRV stress detector use case.

$Type$	$\overline{P}_{Gf1}$	$\overline{P}_{Gf2}$	$\overline{P}_{Bf1}$	$\overline{P}_{Bf2}$	ε [%($\varepsilon_{f1}, \varepsilon_{f2}$)]
1_H	5.28	0.15	5.27	0.16	(0.18,6.66)
1_L	5.05	0.16	4.81	0.17	(4.75,6.25)
Δ	-0.23	+0.01	-0.46	+0.01	
2_H	4.09	0.24	4.29	0.20	(4.88,16.66)
2_L	3.83	0.27	3.45	0.29	(9.92,7.41)
Δ	-0.26	+0.03	-0.84	+0.09	
3_H	5.18	0.16	5.17	0.16	(0.19,0.00)
3_L	4.40	0.19	4.28	0.21	(2.72,10.52)
Δ	-0.78	+0.03	-0.90	+0.05	
4_H	5.27	0.15	5.32	0.15	(0.09,0.00)
4_L	5.16	0.16	5.12	0.17	(0.7,6.25)
Δ	-0.11	+0.01	-0.20	+0.03	
5_H	5.07	0.16	4.82	0.17	(4.93,6.25)
5_L	4.64	0.17	4.63	0.18	(0.21,5.88)
Δ	-0.43	+0.01	-0.19	+0.01	
6_H	4.98	0.16	4.96	0.17	(4.03,6.25)
6_L	4.84	0.17	4.46	0.20	(7.85,17.64)
Δ	-0.14	+0.01	-0.50	+0.03	

except for cases such as 2_H or 6_L, in which strong motion artifacts presented in the signal of BINDI were not cleaned as expected, resulting into locally contaminated segments of signals, which affects directly to the peak detection process and, therefore, to the HRV extraction.

By performing this particular use case, the different detailed trade-offs for rapid-inference applications have been successfully applied. Notwithstanding that the presented use case does not reach the full HRV frequency band detection capability, the goal of rapid stress detection is accomplished using low amount of resources at the expense of frequency resolution.

5. Conclusions

This work provides a detailed DSE for a physiological based constrained wearable device developed by the authors. Different signal processing elements are analyzed and compared based on particular wearable applications needs.

Based on the given DSE results, a particular continuous rapid detection use case is implemented. We demonstrate that stress detection using HRV can be performed by extracting only two frequency bins, which supposes a novel low-power wearable device HRV integration using low-resource, low-complexity computation followed from a detailed DSE.

Certain limitations of the proposed system must be considered. On the one hand, different signal processing techniques can be applied. For instance, to deal with the unevenly spaced HRV data, Lomb-Scargle periodrogram method could be applied [27] instead of FFT. On the other hand, the different possibilities, extension and complexity of the MAR methods lead to not include any specific DSE for this part. This fact must be properly addressed for any physiological wearable constrained device integrating PPG sensors. Moreover, future work related to the inference stage DSE of the affective computing wearable is to be studied and analyzed in further publications.

Some of the limitations identified while performing this work confirms the need for DSEs based on current low-power system-on-chips and physiological signals to be published in the literature.

6. Acknowledgement

This work has been partially supported by the Madrid Region Government, under the Synergic Program EMPATIA-CM, Y2018/ TCS-5046.

References

[1] P. Schmidt, A. Reiss, R. Dürichen, K. V. Laerhoven, Wearable-based affect recognition—a review, Sensors 19 (19) (2019). doi:10.3390/s19194079.
URL https://www.mdpi.com/1424-8220/19/19/4079

[2] L. McCorry, Physiology of the autonomic nervous system, Am. J. Pharm. Educ. (2007) 71–78.

[3] P. Schmidt, A. Reiss, R. Duerichen, C. Marberger, K. Van Laerhoven, Introducing wesad, a multimodal dataset for wearable stress and affect detection, in: Proceedings of the 20th ACM International Conference on Multimodal Interaction, ICMI '18, Association for Computing Machinery, New York, NY, USA, 2018, p. 400–408. doi:10.1145/3242969.3242985.
URL https://doi.org/10.1145/3242969.3242985

[4] L. Shu, J. Xie, M. Yang, Z. Li, Z. Li, D. Liao, X. Xu, X. Yang, A review of emotion recognition using physiological signals, Sensors 18 (2018) 2074. doi:10.3390/s18072074.

[5] B. Appelhans, L. Luecken, Heart rate variability as an index of regulated emotional responding, Review of General Psychology 10 (2006) 229–240. doi:10.1037/1089-2680.10.3.229.

[6] S. D. Kreibig, Autonomic nervous system activity in emotion: A review, Biological Psychology 84 (3) (2010) 394 – 421, the biopsychology of emotion: Current theoretical and empirical perspectives. doi:https://doi.org/10.1016/j.biopsycho.2010.03.010.

[7] K. Georgiou, A. V. Larentzakis, N. N. Khamis, G. I. Alsuhaibani, Y. A. Alaska, E. J. Giallafos, Can wearable devices accurately measure heart rate variability? a systematic review, Folia Medica 60 (1) (2018) 7 – 20.

[8] M. Magno, M. Pritz, P. Mayer, L. Benini, Deepemote: Towards multi-layer neural networks in a low power wearable multi-sensors bracelet, in: 2017 7th IEEE International Workshop on Advances in Sensors and Interfaces (IWASI), 2017, pp. 32–37.

[9] D. Azariadi, V. Tsoutsouras, S. Xydis, D. Soudris, Ecg signal analysis and arrhythmia detection on iot wearable medical devices, in: 2016 5th International Conference on Modern Circuits and Systems Technologies (MOCAST), 2016, pp. 1–4.

[10] S. J. Kang, S. Y. Lee, H. I. Cho, H. Park, Ecg authentication system design based on signal analysis in mobile and wearable devices, IEEE Signal Processing Letters 23 (6) (2016) 805–808.

[11] J. A. Miranda, R. Marino, J. M. Lanza-Gutierrez, T. Riesgo, M. Garcia-Valderas, C. Lopez-Ongil, Embedded emotion recognition within cyber-physical systems using physiological signals, in: 2018 Conference on Design of Circuits and Integrated Systems (DCIS), 2018, pp. 1–6.

[12] E. Rituerto-González, J. A. Miranda, M. F. Canabal, J. M. Lanza-Gutiérrez, C. Peláez-Moreno, C. López-Ongil, A hybrid data fusion architecture for bindi: A wearable solution to combat gender-based violence, in: A. Dziech, W. Mees, A. Czyżewski (Eds.), Multimedia Communications, Services and Security, Springer International Publishing, Cham, 2020, pp. 223–237.

[13] J. A. Miranda, M. F. Canabal, L. Gutiérrez-Martín, J. M. Lanza-Gutiérrez, C. López-Ongil, A design space exploration for heart rate variability in a wearable smart device, in: 2020 XXXV Conference on Design of Circuits and Integrated Systems (DCIS), 2020, pp. 1–6. doi:10.1109/DCIS51330.2020.9268628.

[14] J. A. M. et. al., Embedded emotion recognition: Autonomous multimodal affective internet of things, in: Cyber-Physical Systems Workshop 2018, CPSWS, 2018, pp. 22–29.

[15] S. R. Seydnejad, R. I. Kitney, Real-time heart rate variability extraction using the kaiser window, IEEE Transactions on Biomedical Engineering 44 (10) (1997) 990–1005.

[16] P. V. et. al., Predicting the duration of emotional experience: Two experience sample studies, in: Emotion, Vol. 9, 2009, p. 83.

[17] D. Biswas, N. Simões-Capela, C. Van Hoof, N. Van Helleputte, Heart rate estimation from wrist-worn photoplethysmography: A review, IEEE Sensors Journal 19 (16) (2019) 6560–6570.

[18] L. Sörnmo, P. Laguna, Chapter 7 - ecg signal processing, in: L. Sörnmo, P. Laguna (Eds.), Bioelectrical Signal Processing in Cardiac and Neurological Applications, Biomedical Engineering, Academic Press, Burlington, 2005, pp. 453–566. doi:https://doi.org/10.1016/B978-012437552-9/50007-6.

[19] M. T. Islam, S. Tanvir Ahmed, I. Zabir, C. Shahnaz, S. A. Fattah, Cascade and parallel combination (cpc) of adaptive filters for estimating heart rate during intensive physical exercise from photoplethysmographic signal, Healthcare Technology Letters 5 (1) (2018) 18–24. doi:https://doi.org/10.1049/htl.2017.0027.

[20] J. Lee, M. Kim, H.-K. Park, I. Y. Kim, Motion artifact reduction in wearable photoplethysmography based on multi-channel sensors with multiple wavelengths, Sensors 20 (5) (2020). doi:10.3390/s20051493.
URL https://www.mdpi.com/1424-8220/20/5/1493

[21] F. Li, L. Yang, H. Shi, C. Liu, Differences in photoplethysmography morphological features and feature time series between two opposite emotions: Happiness and sadness, Artery Research 18 (2017) 7–13. doi:https://doi.org/10.1016/j.artres.2017.02.003.
URL https://doi.org/10.1016/j.artres.2017.02.003

[22] Q. Yousef, M. B. I. Reaz, M. Ali, The analysis of ppg morphology: Investigating the effects of aging on arterial compliance, Measurement Science Review 12 (2012) 266–271. doi:10.2478/v10048-012-0036-3.

[23] G. McVeigh, C. Bratteli, D. Morgan, C. Alinder, S. Glasser, S. Finkelstein, J. Cohn, Age-related abnormalities in arterial compliance identified by pressure pulse contour analysis: Aging and arterial compliance, Hypertension 33 (6) (1999) 1392–1398, cited By 286. doi:10.1161/01.HYP.33.6.1392.

[24] F. Foroozan, M. Mohan, J. S. Wu, Robust beat-to-beat detection algorithm for pulse rate variability analysis from wrist photoplethysmography signals, in: 2018 IEEE International Conference on Acoustics, Speech and Signal Processing (ICASSP), 2018, pp. 2136–2140. doi:10.1109/ICASSP.2018.8462286.

[25] M. Soundararajan, S. Arunagiri, S. Alagala, An adaptive delineator for photoplethysmography waveforms, Biomedical Engineering / Biomedizinische Technik 61 (2016) 645 – 655.

[26] H. S. Shin, C. Lee, M. Lee, Adaptive threshold method for the peak detection of photoplethysmographic waveform, Computers in Biology and Medicine 39 (12) (2009) 1145–1152. doi:https://doi.org/10.1016/j.compbiomed.2009.10.006.

[27] J. T. VanderPlas, Understanding the lomb–scargle periodogram, The Astrophysical Journal Supplement Series 236 (1) (2018) 16. doi:10.3847/1538-4365/aab766.
URL https://doi.org/10.3847/1538-4365/aab766